FED - Vol. 14

Computation of Internal Flows: Methods and Applications

FED - Vol. 14

Computation of Internal Flows: Methods and Applications

presented at

ENERGY SOURCES TECHNOLOGY CONFERENCE
NEW ORLEANS, LOUISIANA
FEBRUARY 12-16, 1984

sponsored by

THE FLUID MACHINERY AND FLUID MECHANICS COMMITTEES
FLUIDS ENGINEERING DIVISION, ASME

edited by

PETER M. SOCKOL
NASA LEWIS RESEARCH CENTER

KIRTI N. GHIA
UNIVERSITY OF CINCINNATI

THE AMERICAN SOCIETY OF MECHANICAL ENGINEERS
United Engineering Center 345 East 47th Street New York, N.Y. 10017

Library of Congress Catalog Card Number 83-73578

FOREWORD

With the recent advances in numerical methods and computer technology, an increasing number of internal flows are being simulated on the computer. Because of the broad range of flow conditions and geometries in these flows, a large number of different approaches are being pursued. As a result, objective assessment of the field is difficult. The purpose of this Symposium is to provide a forum for the interchange of ideas and the presentation of new results in the field of numerical methods in fluid mechanics with particular emphasis on computation of internal flows. A second, but no less important goal, is to provide information on the applicability and limitations of these methods.

The Symposium includes three invited lectures. One, by Professor L. S. Langston of the University of Connecticut, is entitled, "Review - Internal Flow Phenomena." The second, by Professors J. J. McGuirk and J. H. Whitelaw of Imperial College of Science and Technology, London, is on "Internal Flows of Relevance to Gas Turbines." The third, by Professor U. Ghia of the University of Cincinnati, is on "Computation of Viscous Internal Flows." There are 18 contributed papers in the Symposium. Some of these are concerned with the application of numerical methods to internal flows such as those in curved ducts or turbomachinery components. The remainder are devoted to new or developing numerical techniques relevant to the analysis of flow in internal passages as well as the design of such passages to achieve a particular objective. The methods range in complexity from two-dimensional viscous-inviscid interaction to three-dimensional solution of the Reynolds-averaged Navier-Stokes equations. The Symposium will conclude with a panel discussion on the "Prospects for Computation of Three-Dimensional Viscous Internal Flows."

The organizers of the Symposium wish to extend their thanks to the authors, session chairmen, reviewers, ASME publication and technical coordination personnel, and the chairmen of the Fluid Machinery and Fluid Mechanics Committees of the ASME Fluids Engineering Division.

Peter M. Sockol
Symposium Co-Chairman

CONTENTS

V. NEW METHODS

COMPUTATION OF VISCOUS FLOWS IN TURBOMACHINERY CASCADES

M. Pouagare,* B. Lakshminarayana,** T. R. Govindan*

Department of Aerospace Engineering
The Pennsylvania State University
University Park, PA 16802

*Graduate Assistant

**Director of Computational Fluid Dynamics Studies and Professor of Aerospace Engineering

ABSTRACT

The space-marching method was used to predict the viscous flow field in turbomachinery cascades. Problems associated with the leading edge stagnation point were overcome by modifying the streamwise pressure gradient term in the momentum equation. Analysis and numerical experiments have proved that for accurate predictions the grid lines in the physical domain must be nearly orthogonal. For staggered cascades a non-periodic grid system was employed, and appropriate approximations were used in the place of the periodicity boundary conditions upstream and downstream of the cascade. The cases tested first were the laminar flow through a flat plate cascade at 45° stagger, and through a symmetric cascade at zero incidence and stagger. The method was then used to predict the turbulent flow through compressor cascades composed of NACA 65-series blades. The predicted drag coefficient, turning angle, boundary layer momentum thicknesses, and velocity profiles were compared with experimental data; the agreement was good in most cases. The solution for any of the cases presented was obtained in less than one minute on an IBM 3081.

NOMENCLATURE

a	angle of attack
b_1, b_2	parameters determining the numerical scheme employed
C	chord
C_D	drag coefficient
C_p	pressure coefficient $(=(p-p_1)/\frac{1}{2}\rho Q_1^2)$
D	diffusion term; drag force
E, E_S, E_P, F, T, P	vectors in the governing equations
e_i	specific internal energy
e	total fluxing energy
J	Jacobian of the grid transformation
k	coefficient of thermal conductivity
ℓ	turbulent length scale in a boundary layer
L	wake semiwidth
M	Mach number
n	streamwise station
p	static pressure
p_s	assumed initial static pressure
Pr	Prandtl number
Q	streamwise velocity
Q_s	velocity defect at the center of the wake
q	dependent vector in the governing equations
r	normal distance from the wall
R_e	Reynolds number $(= Q_1 C/\nu)$
S	vector containing the artificial damping terms
s	spacing
u, v	velocity in the x, y directions, respectively
U	contravariant velocity component along the ξ-coordinate $(= \xi_x u + \xi_y v)$
u_*	friction velocity
V	contravariant velocity component along the η-coordinate $(= \eta_x u + \eta_y v)$
x,y	Cartesian coordinates; x is the axial direction, and y the transverse direction
z	distance from the leading edge measured along the chordline
α	angle of the grid lines with the x-coordinate
β	flow angle (see Fig. 1)
γ	ratio of specific heats
Δm	change in the global mass flow
ΔP_o	total pressure difference across the cascade
δ	boundary layer thickness
ζ	loss coefficient
θ	momentum thickness normalized by C
κ	von Karman constant
λ	stagger angle
μ	molecular viscosity
μ_T	eddy viscosity
ν	kinematic viscosity
ξ, η	body-fitted coordinate system
ξ_x, η_x, ξ_y, η_y	metrics in the grid transformation
ρ	density
σ_1, σ_2, σ_3, σ_4	damping coefficients
ϕ	angle between ξ and η grid lines
ψ_1, ψ_2	viscous dissipation terms in the energy equation
ω	fraction of streamwise pressure gradient kept implicitly

Superscripts

n	streamwise station index
^	vectors in the governing equations in the computational domain

Subscripts

c	correction values
p	quantity at the first grid point away from the wall
ss, ps	suction side, pressure side, respectively
TE	trailing edge values
xy	quantity in (x,y) coordinates
$\xi\eta$	quantity in (ξ,η) coordinates
1, 2	upstream, downstream of the cascade, respectively
∞	quantity at the edge of the boundary layer

INTRODUCTION

A knowledge of the flow field through a cascade of blades is essential for the design of turbomachines. In the early stages of jet engine development, turbomachinery designers depended to a large extent on the experimental data to derive the performance characteristics of cascades. However, experimental data is difficult and time-consuming to obtain. This difficulty has motivated research to predict the performance of cascades with numerical methods.

In the past two decades, considerable progress has been made in the prediction of the inviscid flow through cascades (e.g., Refs. 1, 2). However, much progress has not been made in predicting the viscous flow. The existing time-marching algorithms that can predict the viscous flow are expensive (e.g., Refs. 3,4).

The boundary layer approximation (e.g., Refs. 5, 6), though economical, is difficult to implement in internal flows because of the displacement effects of the boundary layer on the inviscid flow (viscous-inviscid interaction).

This paper presents an economical and accurate algorithm for the prediction of the viscous flow field through turbomachinery cascades. The algorithm is based on the parabolized Navier-Stokes equations, which are solved with the space-marching technique developed by Govindan [7].

The present algorithm requires a knowledge of the streamwise pressure gradient, as the boundary layer approximation does; but, unlike the boundary layer approximation, the present algorithm solves the equations in the entire flow field, and thus the viscous-inviscid interaction problem of boundary layer methods is absent.

Space- (or parabolic-) marching techniques have been widely used for the prediction of the flow through curved channels. However, the prediction of the flow field in cascades presents difficulties that are not found in the prediction of the flow field in curved channels. The most distinct differences are the following:

1. Periodicity of the flow must be enforced upstream and downstream of a cascade.
2. The stagnation point at the leading edge of a cascade causes strong streamwise pressure gradients.
3. The rapid change in the boundary shape near the leading edge of a cascade introduces additional problems.
4. The grid cannot be kept orthogonal everywhere in a cascade.

Some of the problems encountered in the solution of the flow field in curved channels are especially prominent in the case of cascades. These are the following:

1. A strong overall pressure rise (or drop) from inlet to exit.
2. The flow field perceives two distinctly different length scales; the inviscid one (spacing), and the viscous one (boundary layer thickness). To capture both of them a large number of grid points must be used in the transverse direction.
3. A significant part of the flow field is inviscid, and the viscous terms drop out of the equations. Therefore, in that region, the space-marching method is essentially solving the Euler equations. This makes the problem of uncoupled odd and even points, and the resulting numerical instabilities, more severe than in the case where the viscous terms are present.

The above mentioned problems must be overcome for the accurate prediction of the viscous flow field in cascades. These problems as well as ways to overcome them will be discussed in this paper.

The method was first tested in two hypothetical cases. The first case was a flat plate cascade with zero thickness, at zero angle of attack, with space-to-chord ratio of unity, and a stagger angle of 45°. This test case was used to study the problems associated with the stagger angle (non-orthogonal grid), and the periodicity boundary condition. The second test case was a NACA 65-010 cascade with zero inlet and exit flow angles, zero stagger, and space-to-chord ratio of unity. This test case was used to study the problems associated with the large extent of the inviscid region, the leading edge stagnation point, and the rapid changes in the boundary shape near the leading edge.

Finally, the method was tested for cascades used in practice. The predicted exit flow angle, drag coefficient, boundary layer profiles, and boundary layer momentum thicknesses were compared with the available experimental data, and the agreement between them was found to be good.

A modified version of the space-marching code developed by Govindan [7] was used in the computations.

THE GOVERNING EQUATIONS AND THE SPACE-MARCHING METHOD

Details of the technique are given by Govindan [7], and, therefore, only a brief description of the method will be given below. Some modifications to the space-marching code are also described in this section.

The non-dimensionalized steady two-dimensional compressible Navier-Stokes equations can be written in conservation-law form as

$$\frac{\partial E(q)}{\partial x} + \frac{\partial F(q)}{\partial y} = \frac{1}{R_e}\left[\frac{\partial T(q)}{\partial x} + \frac{\partial P(q)}{\partial y}\right] \qquad (1)$$

where

$$q = [\rho,\ \rho u,\ \rho v,\ \rho e_i]^T \tag{2}$$

The vectors E, F, T, P are given the Appendix. Following Govindan [7], the fluxing internal energy (ρe_i) was used instead of the more commonly used total energy e. The use of ρe_i instead of e as an independent variable was found to improve the solution for low Mach number flows.

To facilitate the application of the boundary conditions, a body-fitted coordinate system was used. The body-fitted grid in the physical domain was transformed to a rectangular grid in the computational domain by the transformation

$$\begin{aligned} \xi &= \xi(x,y) \\ \eta &= \eta(x,y) \end{aligned} \tag{3}$$

where ξ is the coordinate in the near-streamwise direction, and η is the coordinate in the transverse direction.

Equation (1) was transformed to the body-fitted coordinate system (ξ,η). The resulting equation can be kept in the same form as Eq. (1),

$$\frac{\partial \hat{E}(q)}{\partial \xi} + \frac{\partial \hat{F}(q)}{\partial \eta} = \frac{1}{Re}\left[\frac{\partial \hat{T}(q)}{\partial \xi} + \frac{\partial \hat{P}(q)}{\partial \eta}\right] \tag{4}$$

where

$$\hat{E} = \frac{\xi_x}{J}E + \frac{\xi_y}{J}F, \qquad \hat{F} = \frac{\eta_x}{J}E + \frac{\eta_y}{J}F,$$

$$\hat{T} = \frac{\xi_x}{J}T + \frac{\xi_y}{J}P, \qquad \hat{P} = \frac{\eta_x}{J}T + \frac{\eta_y}{J}P,$$

and J is the Jacobian of the coordinate transformation given by

$$J = \xi_x\eta_y - \xi_y\eta_x \ . \tag{5}$$

For flows with a dominant flow direction, the Navier-Stokes equations can be parabolized by neglecting the streamwise diffusion terms, and by treating the streamwise pressure gradient in the momentum equation as a source term [7]. Therefore, the Navier-Stokes equations were parabolized by dropping the term $\partial\hat{T}/\partial\xi$ in Eq. (4), and by writing the term $\partial\hat{E}/\partial\xi$ as

$$\frac{\partial \hat{E}}{\partial \xi} = \frac{\partial \hat{E}_s(q)}{\partial \xi} + \hat{E}_p(p_s) \tag{6}$$

where

$$\hat{E}_s(q) = \frac{1}{J}[\rho u,\ \rho uU,\ \rho vU,\ (e+p)U]^T$$

$$\hat{E}_p(p_s) = \frac{1}{J}\frac{p_s^{n+1} - p_s^{n}}{\Delta\xi}[0,\ \xi_x,\ \xi_y,\ 0]^T$$

p_s is the assumed pressure; n is the index in the ξ-direction; n-station is the station at which the solution is being sought.

The parabolized Navier-Stokes equations were written as

$$\frac{\partial \hat{E}_s(q)}{\partial \xi} + \hat{E}_p(p_s) + \frac{\partial \hat{F}(q)}{\partial \eta} = \frac{1}{R_e}\frac{\partial \hat{P}(q)}{\partial \eta} \tag{7}$$

Equation (7) is a well-posed initial value problem that governs the evolution of the flux vector E_s. Starting from an initial η-line, the solution is marched downstream along the ξ direction which is the "time-like" coordinate. The vector $\hat{E}_p(p_s)$ has to be given as an input. In the present investigation, $\hat{E}_p(p_s)$ was estimated from the pressure distribution calculated from an inviscid code.

Modification to the Space-Marching Method for Strong Streamwise Pressure Gradients

In internal flow calculations, the decomposition of E according to Eq. (6) works well only for mild streamwise pressure gradients. In the presence of strong streamwise pressure gradients, part of the streamwise pressure gradient in the momentum equations must be retained in $\hat{E}_s$.

Following an approach similar to Rakich [8], $\hat{E}_s$ and $\hat{E}_p$ were modified as follows:

$$\hat{E}_s = \frac{1}{J}[\rho u,\ \rho uU + \xi_x\omega P,\ \rho vU + \xi_y\omega P,\ (e+P)U]^T \tag{8}$$

$$\hat{E}_p = \frac{(1-\omega)}{J}\frac{p_s^{n+1} - p^{n}}{\Delta\xi}[0,\ \xi_x,\ \xi_y,\ 0]^T \tag{9}$$

where ω is given as in Ref. 9

$$\omega = \gamma M^2/[1 + (\gamma - 1)M^2].$$

Adding and substracting $(1-\omega)p^{n-1}/(\Delta\xi\ J)$ in Eq. (9) and transferring $(1-\omega)(p^n - p^{n-1})/(\Delta\xi\ J)$ into E_s, the following expressions were obtained:

$$\hat{E}_s(q) = \frac{1}{J}[\rho u,\ \rho uU + \xi_x(2\omega-1)P,\ \rho vU + \xi_y(2\omega-1)P,\ (e+P)U]^T \tag{10}$$

$$\hat{E}_p(p_s) = \frac{(1-\omega)}{J}\frac{p_s^{n+1} - p^{n-1}}{\Delta\xi}[0,\ \xi_x,\ \xi_y,\ 0]^T$$

The above form of $\hat{E}_s$ and $\hat{E}_p$ enabled the algorithm to march through regions of strong streamwise pressure gradient (e.g., leading edge region).

The Numerical Technique

Following Beam and Warming [10], Eq. (7) is finite differenced as follows:

$$\left[\left(\frac{\partial \hat{E}_s}{\partial q}\right)^n - \frac{b_1\Delta\xi}{1+b_2}\left[\frac{\partial}{\partial\eta}\left(\frac{\partial B}{\partial q}\right)^n\right]\right]\Delta q^n = \frac{b_2}{1+b_2}\left[\frac{\partial \hat{E}_s}{\partial q}\right]^{n-1}\Delta q^{n-1}$$

$$+ \frac{b_1\ \Delta\xi}{1+b_2}(N^n - N^{n-1}) + \frac{\Delta\xi}{1+b_2}\left[\frac{\partial B}{\partial\eta} + N\right]^n \tag{11}$$

where

$$B = \frac{1}{Re}\frac{\partial \hat{P}}{\partial \eta} - \frac{\partial \hat{F}}{\partial \eta}, \qquad N = -\hat{E}_p, \qquad \Delta q^n = q^n - q^{n-1}$$

The parameters b_1 and b_2 determine the scheme employed. The results in this paper were obtained with $b_1 = 1$, $b_2 = 1/2$ corresponding to a 3-point-backward implicit scheme with truncation error $0(\Delta\xi^3)$.

In order to prevent the uncoupling of the odd and even points, a second order artificial dissipation term was added in Eq. (11) on both the explicit and the implicit side. This term has the form

$$S = \frac{1}{J}\left[\sigma_1 \frac{\partial^2 \rho}{\partial \eta^2}, \sigma_2 \frac{\partial^2 (\rho u)}{\partial \eta^2}, \sigma_3 \frac{\partial^2 (\rho v)}{\partial \eta^2}, \sigma_4 \frac{\partial^2 (\rho e_i)}{\partial \eta^2}\right]^T \qquad (12)$$

where σ_1, σ_2, σ_3, and σ_4 are the damping coefficients. The coefficients σ_2 and σ_3 were carefully chosen so that the damping terms S_2 and S_3 were much smaller than the second order viscous terms.

Global Mass Flow, and Pressure and Velocity Corrections

In calculating a flow field with a space-marching method, an initial velocity profile must be specified at the initial station. This specification determines the global mass flow in an internal flow computation. Furthermore, the streamwise pressure gradient is approximated from the assumed pressure field. However, in an internal flow computation, the specification of the global mass flow, and the streamwise pressure gradient is mutually exclusive. In an internal flow computation where the global mass flow is specified, and the streamwise pressure gradient approximated, requirements of uniqueness of the solution and the linearization errors in the numerical scheme lead to a slow loss of the global mass flow constraint [7]. Maintenance of this constraint is important in internal flow computations, and, therefore, the streamwise pressure gradient must be adjusted to prevent loss of the constraint. In the present algorithm, this is done as follows:

(a) After the solution is found at a particular streamwise station, n, the change in the total mass flow is calculated, and the corrections to the streamwise pressure gradients and the velocity are derived from the following approximate formulae

$$\frac{\Delta P_{sc}}{\Delta \xi} = -\frac{\Delta m}{\int \frac{\xi_x^2 + \xi_y^2}{JU} d\eta}, \qquad u_c = -\frac{\xi_x}{\rho U}\frac{\Delta P_{sc}}{\Delta \xi},$$

$$v_c = -\frac{\xi_y}{\rho U}\frac{\Delta P_{sc}}{\Delta \xi} \qquad (13)$$

(b) The pressure correction is used to correct the streamwise pressure gradient which is going to be used in the solution of the next streamwise station n+1.

(c) The velocity corrections are used to correct the velocity at the current streamwise station n.

The corrections to the pressure gradient and the velocity were found to be small at each streamwise station.

THE GRID SYSTEM

For the numerical solution of the flow field in cascades, the most convenient body-fitted grid is the H-type grid (see Fig. 1). The periodicity boundary

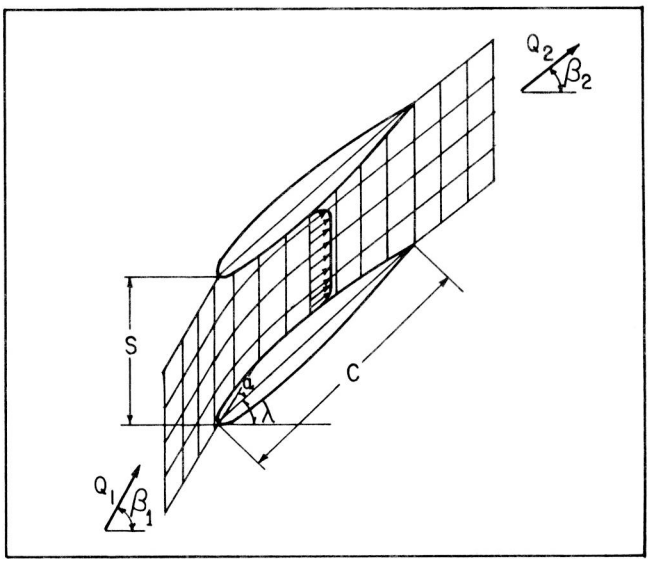

Fig. 1. H-type Periodic Grid and Notation Used

condition upstream and downstream of the cascade requires that the two extremes of the η lines be periodic points. This implies that the ξ and η lines intersect approximately at an angle equal to the stagger angle. The non-orthogonality of ξ and η lines should not present any problems since the transformation expressed by Eq. (3) is general, and no assumption of orthogonality was made. However, only a simplified form of the Navier-Stokes equations is being solved, and the approximations made are not necessarily independent of the coordinate system. In order to see this dependence, consider the flow over a flat plate with the x and ξ coordinates along the flat plate, the y coordinate normal to x and η forming an angle ϕ with ξ (see Fig. 2). For this geometry, the coordinate transformation is given by

$$\xi = x - \cot\phi y$$
$$\eta = y \qquad (14)$$

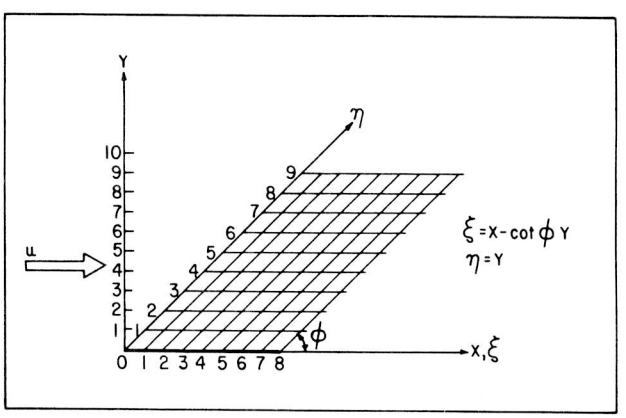

Fig. 2. Non-orthogonal ξ-η Coordinate System for the Flow Over a Flat Plate

Consider the diffusion term in the x-momentum equation for incompressible flow

$$D_{xy} = \frac{1}{Re}\left[\frac{\partial^2 u}{\partial x^2} + \frac{\partial^2 u}{\partial y^2}\right] . \qquad (15)$$

The xy index indicates that the diffusion D is considered in the x,y coordinate system.

Transforming Eq. (15) to (ξ,η) coordinates, and assuming that all metrics are constant throughout the domain of interest, the following expression is obtained:

$$D_{\xi\eta} = \frac{1}{Re}\left[\left(\xi_x^2 + \xi_y^2\right)\frac{\partial^2 u}{\partial \xi^2} + \left(\eta_x^2 + \eta_y^2\right)\frac{\partial^2 u}{\partial \eta^2} + 2(\xi_x\eta_x + \eta_y\xi_y)\frac{\partial}{\partial \xi}\left[\frac{\partial u}{\partial \eta}\right]\right] . \qquad (16)$$

After neglecting the streamwise diffusion terms, $D_{\xi\eta}$ becomes

$$D^*_{\xi\eta} = \frac{1}{Re}\left(\eta_x^2 + \eta_y^2\right)\frac{\partial^2 u}{\partial \eta^2} . \qquad (17)$$

When $D_{\xi\eta}$ is transformed back to (x,y) coordinates, D_{xy} will be obtained as given by Eq. (15). However, transforming $D^*_{\xi\eta}$ back to (x,y) coordinates, the following expression is obtained:

$$D^*_{xy} = \frac{1}{ReJ^2}\left[\left(\eta_x^2\xi_y^2 + \eta_y^2\xi_y^2\right)\frac{\partial^2 u}{\partial x^2} + \left(\eta_y^2\xi_x^2 + \xi_x^2\eta_x^2\right)\frac{\partial^2 u}{\partial y^2} - 2\left(\eta_x^2 + \eta_y^2\right)\xi_x\xi_y\frac{\partial^2 u}{\partial x\partial y}\right] \qquad (18)$$

For the particular example of the flat plate (Fig. 2), Eq. (18) becomes

$$D^*_{xy} = \frac{1}{Re}\left[(\cot\phi)^2\frac{\partial^2 u}{\partial x^2} + \frac{\partial^2 u}{\partial y^2} + 2\cot\phi\,\frac{\partial^2 u}{\partial x\partial y}\right] . \qquad (19)$$

Equation (19) indicates that, depending on the angle ϕ, part of the streamwise diffusion is retained in D^*_{xy} and $D^*_{\xi\eta}$. Only when $\phi = 90°$ (i.e. when ξ,η is an orthogonal coordinate system), the streamwise diffusion terms in D^*_{xy} and $D^*_{\xi\eta}$ are zero.

A similar analysis of the streamwise pressure gradient term [11] showed that the assumption made concerning this term is strictly valid only for an orthogonal (ξ,η) grid system. Therefore, the basic assumptions used to parabolize the Navier-Stokes equations do not hold for a non-orthogonal grid system.

Numerical experiments on the laminar flow on a flat plate (Fig. 2) indicated that the solution depended on the angle ϕ, and that the correct solution (Blasius solution) was obtained only with $\phi = 90°$.

In a recent publication, Degani and Steger [12] compared the results of the thin Navier-Stokes equations with those of the full Navier-Stokes equations for the flow over a ramp. They indicated in their paper that the agreement between the two remained good only when the ξ and η lines intersected at an angle greater than 70°.

As has been shown, it is important to keep the ξ and η lines as close to being orthogonal as possible. For the flow through staggered cascades, this requires the use of a non-periodic grid. In the present investigation, a non-periodic grid is generated algebraically as follows (see Fig. 3):

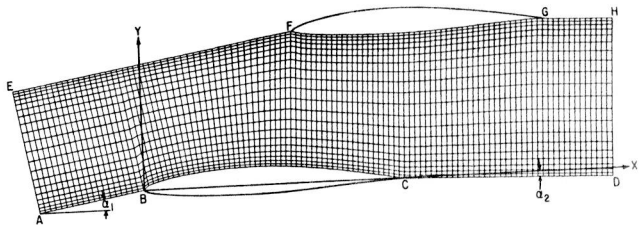

Fig. 3. H-type Non-periodic Grid

1. The x-coordinate is aligned with the chordline.
2. The lower boundary is formed by a straight line AB forming an angle α_1 with the x-axis, the suction side of the airfoil BC, and a second straight line CD forming an angle α_2 with the x-axis.
3. The upper boundary is formed by a straight line EF parallel to AB, the pressure side of the airfoil FG, and a second straight line GH parallel to CD.
4. The η-lines are straight lines. They are drawn normal to the lower surface along AB and CD. Along BC, the η lines are drawn normal to the suction surface wherever the slope of the surface $\tan\alpha$ satisfied the condition

   $$\tan\alpha_2 \leq \tan\alpha \leq \tan\alpha_1 .$$

   If $\tan\alpha > \tan\alpha_1$, the η-lines are drawn parallel to the normal on AB, and if $\tan\alpha < \tan\alpha_2$, the η-lines are drawn parallel to the normal on CD.
5. The angle α_1 need not be related to the flow direction; α_1 is that angle that permits most η-lines to be normal to the ξ-lines. The angle α_2 is more difficult to find; it has to follow the direction of the exit flow. A detailed discussion on α_2 follows in the boundary condition section.
6. The spacing in the η direction is found. Grid points are clustered near the two extremes of the η-lines through an exponential function. When the spacing in the η direction is found, the ξ-lines are drawn.

The grid system generated by the above method is nearly orthogonal in the whole domain except in the immediate vicinity of the leading edge.

INITIAL AND BOUNDARY CONDITIONS

Initial Conditions

The required inviscid pressure distribution for calculating $\hat{E}_p(p_s)$ is obtained from a modified version of Douglas-Neumann cascade program [13]. The space-marching solution starts from the initial line AE as shown in Fig. 4. All the required quantities (ρ,u,v,p) are obtained from the inviscid solution. The present method does not capture the elliptic effects. These are all included in the initial pressure distribution

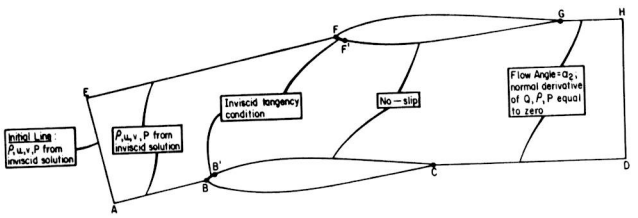

Fig. 4. Boundary Conditions for the Non-Periodic Grid

prescribed. Therefore, the calculation need not start from far upstream of the leading edge. The solution can start from anywhere upstream of the leading edge or even just at the leading edge.

Boundary Conditions Upstream of the Leading Edge

The most appropriate boundary condition upstream of the leading edge is the periodicity condition. However, the grid system employed does not allow for the application of the precise periodic boundary condition. In the region of the boundary lines AB and EF, the viscous effects are negligible, and, therefore, the known inviscid values of velocity, pressure, and density are used on these lines as boundary conditions. The periodicity condition is thus satisfied since the inviscid solution is periodic.

Boundary Conditions on the Blade Surfaces

In a viscous calculation, no-slip boundary condition must be used on solid surfaces. However, in the present investigation the tangency inviscid condition was used near the leading edge (BB' and FF' in Fig. 4). The flow in the interior points does not follow the rapid change of the boundary shape, if the no-slip condition is applied in this region. The extent of BB' and FF' is approximately 5 percent of the chord. Downstream of B' and F', the no-slip boundary condition is used for laminar flow, and a slip condition for turbulent flow. The latter is discussed in the turbulence model section. The use of an inviscid boundary condition during the initial 5 percent of the chord does not affect the final solution since the boundary layer thickness in this region is smaller than the distance between the wall and the first grid point away from the wall.

Boundary Conditions Downstream of the Trailing Edge

The most appropriate boundary condition downstream of the trailing edge is the periodicity condition. However, as upstream of the leading edge, the grid system employed does not allow for the application of the precise periodic boundary condition. The problem downstream is more severe than upstream of the cascade, since the inviscid solution cannot be used because of the presence of the wake in this region. Instead, the lines CD and GH are chosen to be along the exit flow direction, estimated from experimental data, or from the inviscid solution, or from correlations. The normal derivative of the streamwise velocity, density, and pressure is zero along DC and GH

$$\frac{\partial \rho}{\partial r} = \frac{\partial p}{\partial r} = \frac{\partial Q}{\partial r} = 0 \ .$$

TURBULENCE CLOSURE MODEL

In order to model the effects of turbulence, Prandtl's mixing-length hypothesis is used for the boundary layer and the wake.

For the boundary layer, the eddy viscosity is calculated from the formula,

$$\mu_T = \rho \ell^2 [\frac{\partial Q}{\partial r}] R_e \quad \text{with} \quad \begin{aligned} \ell &= \kappa r \quad \text{for } r/\delta \leq 0.219 \\ \ell &= 0.09\delta \quad \text{for } r/\delta > 0.219 \end{aligned} \tag{20}$$

where Q the streamwise velocity, r the normal distance from the wall, and κ the von Karman constant ($\kappa = 0.41$). For the wake, μ_T is calculated from the formula [14]

$$\mu_T = \rho c L Q_S R_e \quad \text{with} \quad c = 0.094 \tag{21}$$

where Q_S is the velocity defect at the center of the wake, and L the wake semi-width; L is defined as the distance between the center of the wake and the point where the velocity defect is equal to $Q_S/2$.

The calculation of the eddy viscosity is lagged one streamwise step. The mean flow equations are first solved at station n using the eddy viscosity derived at the previous station n-1. The derived mean flow quantities at station n are then used to calculate the eddy viscosity to be used at station n+1.

In order to avoid the use of a large number of grid points near the wall, a wall function is used to estimate a slip velocity. Following Kreskowsky et al. [15], the wall slip velocity is derived by assuming that the velocity profile is logarithmic at the first grid point away from the wall. Therefore, the velocity gradient at the first grid point away from the wall is given by

$$\frac{\partial Q_p}{\partial r} = \frac{u_*}{\kappa r_p} \ . \tag{22}$$

The index p indicates quantities at the first grid point away from the wall. Using a backward finite difference, the wall slip velocity is estimated from Eq. (22) as

$$Q_{SLIP} = Q_p - \frac{u_*}{\kappa} \ . \tag{23}$$

The friction velocity u_* is found from the law of the wall written at the first grid point away from the wall;

$$\frac{Q_p}{u_*} = \frac{1}{\kappa} \ln(9 \frac{u_* r_p}{\nu} R_e) \ . \tag{24}$$

The first grid point away from the wall is chosen such that it is outside the laminar sublayer, and in the law of the wall region.

RESULTS AND DISCUSSION

Flat Plate Cascade at 45° Stagger

The method was first tested for the laminar flow ($R_e = 10^4$) through a flat plate cascade with zero thickness, at zero angle of attack, space-to-chord ratio of unity, and a stagger angle of 45°. For such a cascade, the inviscid flow solution gives a uniform pressure everywhere, and thus, if the boundary layer approximation is employed, the viscous solution is given by the Blasius solution.

When the periodic grid (ξ and η lines intersecting at 45°) was used in the solution, the growth of the boundary layer on the lower surface was very different from the growth on the upper surface, and both were very different from the Blasius solution. This resulted from the non-orthogonality of the grid. The growth of the boundary layer was very different on the two surfaces, because the term $2\cot\phi\partial^2 u/\partial x\partial y$ in Eq. (21) had a different sign on each surface (ϕ = 45° on the lower surface, and ϕ = 135° on the upper surface).

The axial velocity profiles obtained with the non-periodic grid are compared with the Blasius solution in Fig. 5. One hundred streamwise steps per chord-

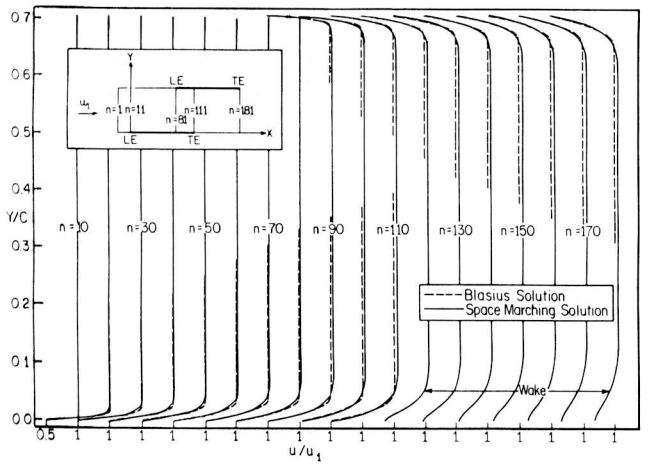

Fig. 5. Axial Velocity Profiles in a Flat Plate Cascade at 45° Stagger

length, and 49 grid points in the η direction were used in the computation. Fig. 5 shows that the present solution captures the acceleration of the core flow resulting from the development of the boundary layers on the two surfaces. Considering that there are only 2 to 12 grid points in the boundary layer, the results of the space-marching method are reasonably close to Blasius solution if the acceleration of the core flow is neglected.

Symmetric Cascade

The method was next tested for the laminar flow ($R_e = 10^4$) through a cascade composed of NACA 65-010 airfoils, with zero inlet and exit flow angles, zero stagger, and space-to-chord ratio of unity. One hundred steps per chord-length, and 49 grid points in the η direction were used in the computation. Fig. 6 shows the predicted axial velocity profiles as well as those obtained from Douglas-Neumann inviscid code [13]. The space-marching method responds well to the strong streamwise pressure gradients present near the leading edge, and it captures the acceleration of the core flow resulting from the development of the boundary layers on the two surfaces.

Figure 7 shows the calculated velocity vectors. The flow follows the boundary shape everywhere, including the leading edge region.

Herrig et al.'s Cascade [16]

The turbulent flow through a cascade composed of NACA 65-010 airfoils, experimentally tested by Herrig

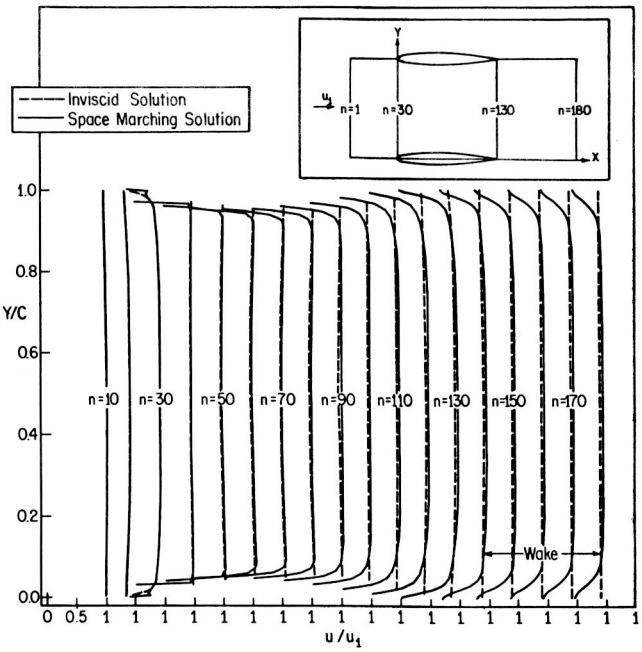

Fig. 6. Axial Velocity Profiles in a Symmetric Cascade

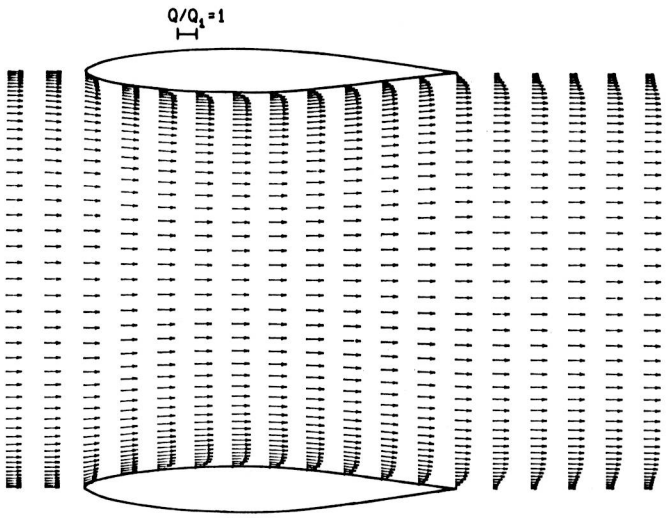

Fig. 7. Velocity Vectors in a Symmetric Cascade

et al. [16], was computed with the present method at two different angles of attack (a = 4°, 8°). The parameters of the two cases were as follows:

Angle of Attack	4°	8°
Inlet Flow Angle	30°	30°
Space-to-Chord Ratio	1	1

Two hundred steps per chord-length, and 49 grid points in the η direction were used in the calculation.

The predicted momentum thicknesses on both surfaces at the two angles of attack are shown in Fig. 8.

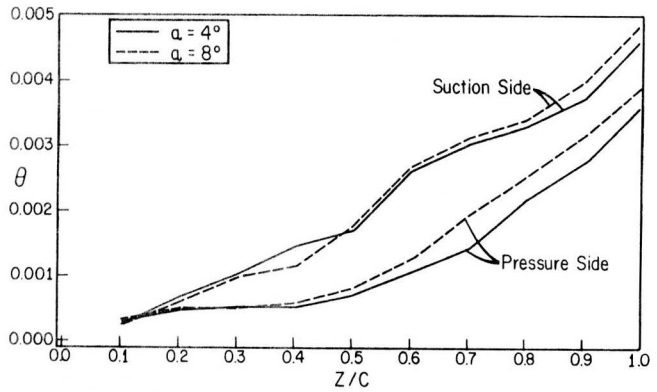

Fig. 8. Boundary Layer Momentum Thickness in Herrig et al.'s Cascade [16]

Using the predicted momentum thicknesses at the trailing edge, the loss coefficient ζ was calculated from Speidel's [17] formula

$$\zeta = \frac{\Delta P_o}{\frac{1}{2}\rho Q_1^2} = \frac{2(\theta_{ss} + \theta_{ps})_{TE}}{\cos^3\beta_2 \cos^{-2}\beta_1} \left(\frac{C}{s}\right) . \qquad (25)$$

Then, the drag coefficient was calculated from the relationship

$$C_D = \frac{D}{\frac{1}{2}\rho Q_1^2 C} = \zeta\left(\frac{s}{c}\right) \cos\beta_m \qquad (26)$$

where $\beta_m = (\tan\beta_1 + \tan\beta_2)/2.$

The predicted C_D as well as the predicted turning angle are compared with the measured ones in Table 1. The agreement between predicted and measured values is good. The differences in the values of C_D cannot be considered high since C_D is a small, and difficult to measure quantity.

Table 1. Predicted and Measured C_D and $\beta_2-\beta_1$ for a NACA 65-010 Cascade

a	C_D Measured	C_D Predicted	$\beta_2 - \beta_1$ Measured	$\beta_2 - \beta_1$ Predicted
4°	0.0125	0.0152	3°	2.5°
8°	0.0125	0.0150	7°	6.6°

Peterson's Cascade [18]

Peterson measured the boundary layer developing on a cascade composed of NACA 65-410 airfoils. The parameters of the cascade were as follows: a = 10°, λ = 45°, s/c = 0.85.

Two hundred steps per chord-length and 49 grid points in the η direction were used in the calculation. The solution was started at 5 percent of the chord-length downstream of the leading edge on the lower surface (see insert in Fig. 9).

The predicted streamwise velocity profiles as well as those obtained from the Douglas-Neumann inviscid code are shown in Fig. 9. This figure shows that the viscous effects alter the inviscid velocity distribution. This is prominent at the trailing edge region.

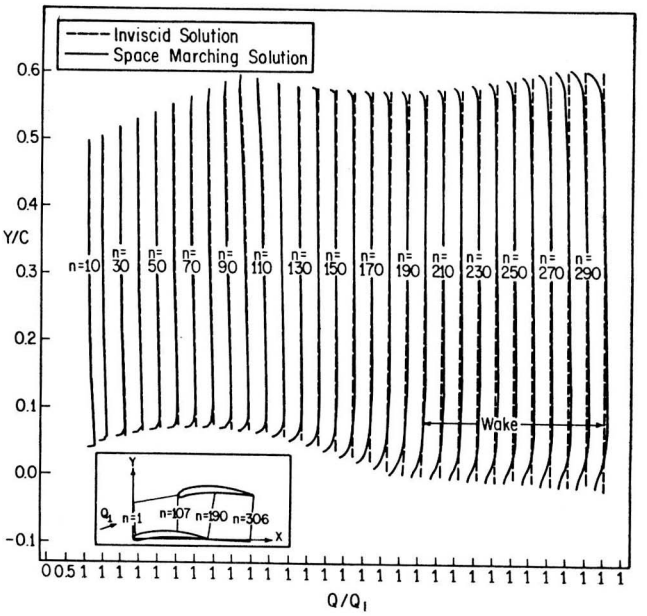

Fig. 9. Streamwise Velocity Profiles in Peterson's Cascade [18]

The predicted boundary layer profiles on the suction and the pressure sides are compared with those measured in Figs. 10 and 11, respectively. The agreement between the two is good on the suction side. However, on the pressure side, the agreement is good only at z/C = 0.9. The data at the last three locations on the pressure side (z/C = 0.8, 0.9, 0.98) does not seem correct since the velocity defect near the wall decreases with z/C increasing.

The predicted and measured momentum thicknesses are compared in Fig. 12. The agreement is good up to 80 percent of the chord.

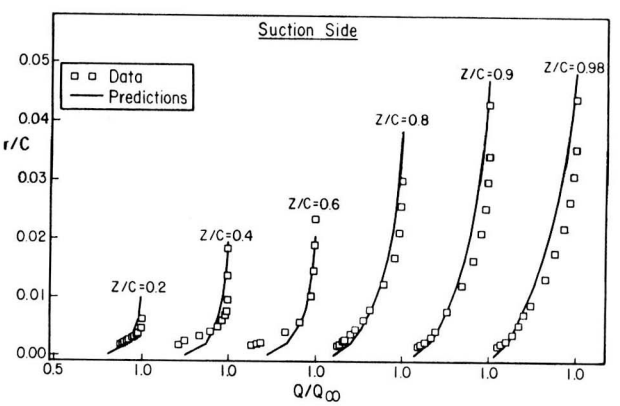

Fig. 10. Boundary Layer Profiles on the Suction Side of Peterson's Cascade

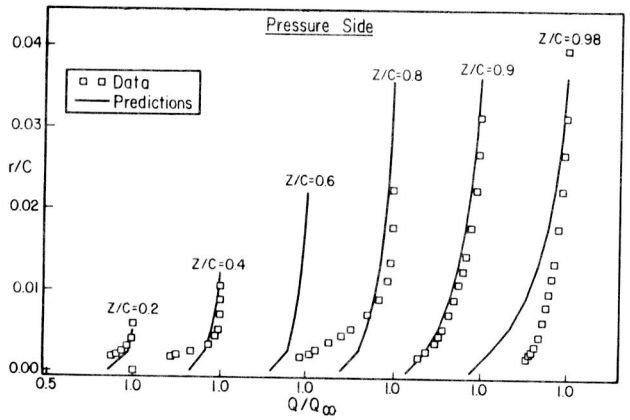

Fig. 11. Boundary Layer Velocity Profiles on the Pressure Side of Peterson's Cascade

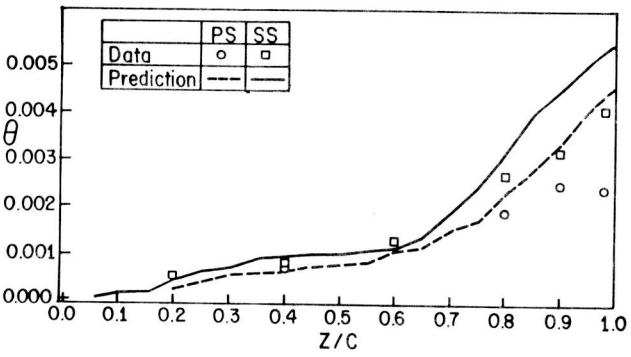

Fig. 12. Boundary Layer Momentum Thickness in Peterson's Cascade

One possible reason for the discrepancies between the predicted and the measured values is the inaccurate initial inviscid pressure distribution. Fig.13 shows the measured blade pressure distribution as well as that predicted from the Douglas-Neumann program. The pressure gradients are comparable only on the suction side up to 80 percent of the chord. The results of the space-marching code can be improved, if a more accurate initial pressure distribution is available.

CONCLUDING REMARKS

The present investigation has demonstrated that the space-marching method can predict the viscous flow in turbomachinery cascades. By keeping part of the streamwise pressure gradient implicitly in the calculation, the method was able to go through regions of strong streamwise pressure gradients, such as the leading edge region. The necessity of keeping the grid nearly orthogonal has been demonstrated. A nearly orthogonal, non-periodic grid system for cascades has been proposed along with the boundary conditions that must be used. Second order artificial damping terms were used to avoid the uncoupling of the odd and even points in the inviscid region of the flow field.

The method is economical; the solution for Peterson's cascade on a 306 x 49 grid was obtained in about 50 sec on an IBM 3081. The accuracy of the

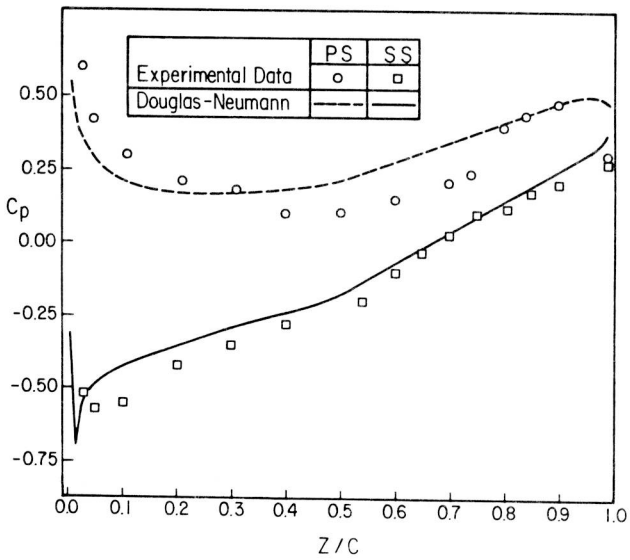

Fig. 13. Blade Pressure Distribution in Peterson's Cascade

method is good, but it can be improved by using a more accurate initial pressure distribution.

Even though the test cases presented in this paper were all for incompressible flows, the method and the code can be used also for the prediction of compressible flows.

ACKNOWLEDGMENT

This investigation was carried out under the sponsorship of the National Aeronautics and Space Administration, through the Grant NSG 3266, with Dr. P. M. Sockol as the Technical Monitor.

REFERENCES

1. Denton, J. D., "A Time-Marching Method for Two- and Three-Dimensional Blade-to-Blade Flow," Aeronautical Research Council R&M 3775, 1975.

2. McFarland, E. R., "Solution of Plane Cascade Flow Using Improved Surface Singularity Methods," NASA TM 81589, 1981.

3. Steger, J. L., Pulliam, T. H., and Chima, R. V., "An Implicit Finite-Difference Code for Inviscid and Viscous Cascade Flows," AIAA Paper 80-1427, AIAA 13th Fluid and Plasma Dynamics Conference, Snowmass, 1980.

4. Shamroth, S., Gibeling, H. J., and McDonald, H., "A Navier-Stokes Solution for Laminar and Turbulent Flow Through a Cascade of Airfoils," AIAA Paper 80-1426, AIAA 13th Fluid and Plasma Dynamics Conference, Snowmass, 1980.

5. Sharma, O. P., Wells, R. A., Schlinter, R. H., and Bailey, D. A., "Boundary Layer Development on Turbine Airfoil Suction Surfaces," Journal of Engineering for Power, Vol. 104, No. 3, July 1982, pp. 689-706.

6. Lakshminarayana, B., and Govindan, T. R., "Analysis of Turbulent Boundary Layer on Cascade and Rotor Blades of Turbomachinery," AIAA Journal, Vol. 19, No. 10, 1981, pp. 1333-1341.

7. Govindan, T. R., "A Space-Marching Method for the Navier-Stokes Equations for Internal Flows," Ph.D. Thesis, Department of Aerospace Engineering, The Pennsylvania State University, 1983.

8. Rakich, J. V., "Iterative PNS Method for Attached Flows With Upstream Influence," AIAA Paper No. 83-1955, 1983.

9. Vigneron, Y. C., Rakich, J, V., and Tannehill, J. C., "Calculation of Supersonic Viscous Flow Over Delta Wings With Sharp Subsonic Leading Edges," NASA TM-78500, 1978.

10. Beam, R. M., and Warming, R. F., "An Implicit Factored Scheme for the Compressible Navier-Stokes Equations," AIAA Journal, Vol. 16, No. 4, 1978.

11. Pouagare, M., "Numerical and Experimental Investigation of the Compressor Rotor Flow Field," Ph.D. Thesis (in preparation), Department of Aerospace Engineering, The Pennsylvania State University, 1984.

12. Degani, D., Steger, J. L., "Comparison Between Navier-Stokes and Thin-Layer Computations for Separated Supersonic Flow," AIAA Journal, Vol. 21, No. 11, 1983.

13. Yocum, A. M., "A Computer Program for Calculating Potential Flow Solutions for Flow Through Linear and Stationary Circular Cascades," TM-81-130, Applied Research Laboratory, The Pennsylvania State University.

14. Schlichting, H., Boundary-Layer Theory, McGraw-Hill Book Company, 7th edition, 1979.

15. Kreskovsky, J. P., Briley, W. R., and McDonald, H., "Turbofan Forced Mixer-Nozzle Internal Flow Field," NACA CR-3494, 1982.

16. Herrig L. J., Emery, J. C., Erwin, J. R., "Systematic Two-Dimensional Cascade Tests of NACA 65-series Compressor Blades at Low Speeds," NACA TN 3916, 1957.

17. Speidel, L., "Berechrung der Strömungverluste von ungestaffelten Ebenen Schaufelgittern," Ing. Arch., 22, 295, 1954.

18. Peterson, C. R., "Boundary Layer on an Airfoil in a Cascade," MIT Report No. 49, Dec. 1958.

APPENDIX

The vectors E, F, T, P in Eq. (1) are given by the following expressions:

$$E = \begin{bmatrix} \rho u \\ \rho u^2 + p \\ \rho uv \\ (e + p)u \end{bmatrix} \qquad F = \begin{bmatrix} \rho v \\ \rho uv \\ \rho v^2 + p \\ (e + p)v \end{bmatrix}$$

$$T = \begin{bmatrix} 0 \\ 2\mu \frac{\partial u}{\partial x} - \frac{2}{3}\mu\left(\frac{\partial u}{\partial x} + \frac{\partial v}{\partial y}\right) \\ \mu\left(\frac{\partial v}{\partial x} + \frac{\partial u}{\partial x}\right) \\ \frac{k\gamma}{Pr}\frac{\partial e_i}{\partial x} + \psi_1 \end{bmatrix}$$

$$P = \begin{bmatrix} 0 \\ \mu\left(\frac{\partial u}{\partial y} + \frac{\partial v}{\partial x}\right) \\ 2\mu \frac{\partial v}{\partial y} - \frac{2}{3}\mu\left(\frac{\partial u}{\partial x} + \frac{\partial v}{\partial y}\right) \\ \frac{k\gamma}{Pr}\frac{\partial e_i}{\partial y} + \psi_2 \end{bmatrix}$$

where ψ_1 and ψ_2 compose the viscous dissipation terms in the energy equation and are given by

$$\psi_1 = 2\mu u \frac{\partial u}{\partial x} - \frac{2}{3}\mu u\left(\frac{\partial u}{\partial x} + \frac{\partial v}{\partial y}\right) + \mu v\left(\frac{\partial u}{\partial y} + \frac{\partial v}{\partial x}\right)$$

$$\psi_2 = 2\mu v \frac{\partial v}{\partial y} - \frac{2}{3}\mu v\left(\frac{\partial u}{\partial x} + \frac{\partial v}{\partial y}\right) + \mu u\left(\frac{\partial v}{\partial x} + \frac{\partial u}{\partial y}\right) .$$

The equation of state for a perfect gas closes the above system of equations and can be written as follows:

$$p = (\gamma - 1)\rho e_i$$

with

$$e_i = \frac{e}{\rho} - \frac{1}{2}(u^2 + v^2).$$

THE RULE OF FORBIDDEN SIGNALS AND APPARENT MACH NUMBER IN TRANSONIC COMPRESSOR CASCADES

David C. Prince, Jr.
Consulting Engineer
Aircraft Engine Business Group
General Electric Company
Cincinnati, Ohio 45215

ABSTRACT

A large body of experimental data from supersonic compressors is reviewed and common operational characteristics identified. Overall flow characteristics and suction surface leading edge behavior show that the "Rule of Forbidden Signals" is a relevant fundamental principle. The "Rule of Forbidden Signals" is usually circumvented over much of the airfoil pressure surfaces; the circumstances often suggest a reduced "apparent Mach number". Circumstances surrounding appearance and disappearance of secondary shocks also suggest the idea of the reduced "apparent Mach number". Two-dimensional Method of Characteristics analyses are useful tools for understanding the observations, provided appropriate allowance for a third dimension influence on streamtube cross section area is made. If radial equilibrium against the centrifugal forces of absolute swirl is implemented in a reliable and recognizable manner, a means for justifying the apparent streamtube areas seems attainable.

Introduction

Reference 1 presented a status report on experimental observations on shock structures in transonic compressors, including quotations of the frustrations encountered by investigators into the subject. The subject continues to generate much interest, with many papers presented at sessions of the technical society meetings devoted to cascade and turbomachinery aerodynamics. New experimental data have been presented in References 2-7. New results on analytical modeling of the flow in compressor rotors have been presented in References 5-10.

Reference 1 summarized the results of its investigations in a tabulation of observations, which could serve as a checklist of phenomena to be used to evaluate new experience. More recent experience has suggested revisions of the tabulation. The new tabulation, Table I, serves as a framework for evaluating the data discussed in this paper.

There are three principal objectives of this paper.

The first of these objectives is to examine the upstream propagation of pressure disturbances in transonic compressors for consistency with the "Rule of Forbidden Signals". In elementary supersonic flow analysis pressure signals cannot, of course, propa-

Table I. Transonic Compressor Flow Pattern Observations.

1. Upstream flow is isolated from a downstream throttle; throttling is uniform over the annulus.
2. Shock waves appear upstream of compressor rotors and compressor cascades.
3. Attached shock wave angles within rotor cascade passages approximate maximum deflection.
4. Shock discontinuities are substantially below expectation.
5. Passage and downstream shocks disappear at supersonic pressure levels.
6. Leading edge shocks are mostly absorbed at incidence on suction surface.
7. Flow induction suction surfaces respect "Forbidden Signals".
8. "Forbidden Signals" are circumvented on pressure surfaces (except possibly for 20% chord near leading edge).
9. Passage exit pressure and velocity levels imply substantially reduced flow area.